Ship-of-opportunity noise inversions for geoacoustic profiles of a layered mud-sand seabed

D. Tollefsen, S. E. Dosso, and D. P. Knobles

Submitted : March 11, 2019
Received :
Running title : Ship-noise inversions for geoacoustic profiles

D. Tollefsen is with the Norwegian Defence Research Establishment (FFI), Defence Systems Division, NO-3191 Horten, Norway (e-mail: dag.tollefsen@ffi.no).

S. E. Dosso is with the School of Earth and Ocean Sciences, University of Victoria, Victoria, British Columbia, Canada V8W 3P6 (e-mail: sdosso@uvic.ca)

D. P. Knobles is with Knobles Scientific and Analysis, Austin, Texas 78755, USA (e-mail: dpknobles@kphysics.org)

DOI til publisert versjon/DOI to published version: 10.1109/JOE.2019.2908026

***Abstract*—** This paper considers the use of broadband noise from a ship–of-opportunity in statistical inference for estimating geoacoustic parameters of a layered mud-sand seabed model via trans-dimensional (trans-D) Bayesian matched-field inversion, with applications to data collected with a bottom-moored horizontal array in the 2017 Seabed Characterization Experiment conducted on the New England Shelf. The trans-D approach applied here samples probabilistically over possible model parameterizations (different numbers of seabed layer interfaces), and provides quantitative uncertainty estimates of seabed geoacoustic profiles. Inversions are carried out for acoustic data sets collected both when the ship-of-opportunity (a container ship) was oriented with its bow and with its stern towards the array. A third inversion involved combining data from a series of segments along the ship track. Inversion results image an upper sediment layer 3–7 m thick with low sound speed (close to the water sound speed) over higher-speed sediment, with indication of a transition layer above the interface. Sediment parameter estimates from the inversions are in good agreement with direct measurements from sediment cores and other geophysical data collected in the experiment area.

Index Terms— Geoacoustic inversion, ship-noise inversion, surface ship radiated noise, trans-dimensional inversion

DOI til publisert versjon/DOI to published version: 10.1109/JOE.2019.2908026

I. INTRODUCTION

The use of noise from ships [1]–[7] and natural noise sources [8], [9] to infer geoacoustic properties of the seabed has attracted wide research interest over the past decade. Most of this work has been conducted in areas where the seabed is composed of predominantly sandy sediments, for which the sediment sound speed is well above the sound speed in water. Environments where the seabed (at least the upper layers) is of a predominantly fine-grained sediment type (e.g., mud) with much lower sound speeds have been received much less attention to date.

The 2017 Seabed Characterization Experiment (SBCEX17), a large coordinated multi-instrument/multi-institutional experiment sponsored by the Office of Naval Research, was carried out in the New England *Mud Patch* in March and April, 2017 [10]. The stated goals of this experiment included assessing geoacoustic models and inversion methods, and quantifying model parameter uncertainties at the Mud Patch site. This paper addresses these goals for ship-noise inversion. As part of this experiment, the Norwegian Defence Research Establishment (FFI) deployed a horizontal line array (HLA) of hydrophones at the seabed within 2 nmi (3.7 km) from a commercial shipping lane leading to the Port of New York and New Jersey. This provided an opportunity to collect broadband noise data sets from large commercial ships to examine the use of ship noise for geoacoustic inversion of muddy seabeds. Previous ship-noise inversion studies have been applied to noise due to small research ships (lengths 33 m to 93 m, moving at speeds of 8 kts or less); the present work is, to our knowledge, the first application to noise from a large commercial ship-of-opportunity (335 m in length moving at 18 kts) for this purpose. Data sets considered here include noise radiated from a container ship at bow and at stern aspect, as well as simultaneous inversion of data from multiple time segments along a track.

Matched-field geoacoustic inversion of ship-noise data is carried out here with a trans-dimensional (trans-D) Bayesian formulation [11]–[13] to provide parameter estimation and uncertainty quantification for a layered seabed model. Trans-D inversion considers the number of seabed layer interfaces as an unknown, sampled probabilistically in the inversion. This allows the data to determine the number and

DOI til publisert versjon/DOI to published version: 10.1109/JOE.2019.2908026

depths of sediment interfaces, concentrating model structure where it is required while maintaining a parsimonious solution. Further, the uncertainty in the parameterization (number of interfaces) is quantified and included in the geoacoustic parameter uncertainties.

The remainder of this paper is organized as follows. Section II describes the experiment, geophysical and acoustic data, and the geoacoustic and source models used in the inversions. Section III provides a brief overview of trans-D inversion and the method applied in this work. Section IV presents results in terms of parameter and uncertainty estimates of seabed model parameters (sediment geoacoustic profiles) from the inversions, and compares these estimates with direct measurements from sediment cores and other geophysical data collected in the experiment area. Section V summarizes this paper.

II. EXPERIMENT, DATA, AND MODEL

SBCEX17 took place in an area known as the New England Mud Patch [10]; see Fig. 1 for the location. The FFI array was deployed by the R/V *Neil Armstrong* on the seabed in an east-west orientation in the north-east (NE) corner of the experiment area (black line in Fig. 1). An earlier geophysical (pilot) survey was conducted from the R/V *Sharp* in July–August, 2015, and provided information on bathymetry and seabed structure [10]. A towed EdgeTech SB-0512i sonar (frequency range 500 Hz – 12 kHz) was used for subbottom profiling. In addition, a number of sediment cores were collected in the pilot survey and in a subsequent coring survey carried out in April–May, 2016. Sediment coring instruments included a vibracore and a piston coring system operated by the U. S. Geological Survey and the Naval Research Laboratory. The locations of the cores are indicated with dots in Fig. 1.

DOI til publisert versjon/DOI to published version: 10.1109/JOE.2019.2908026

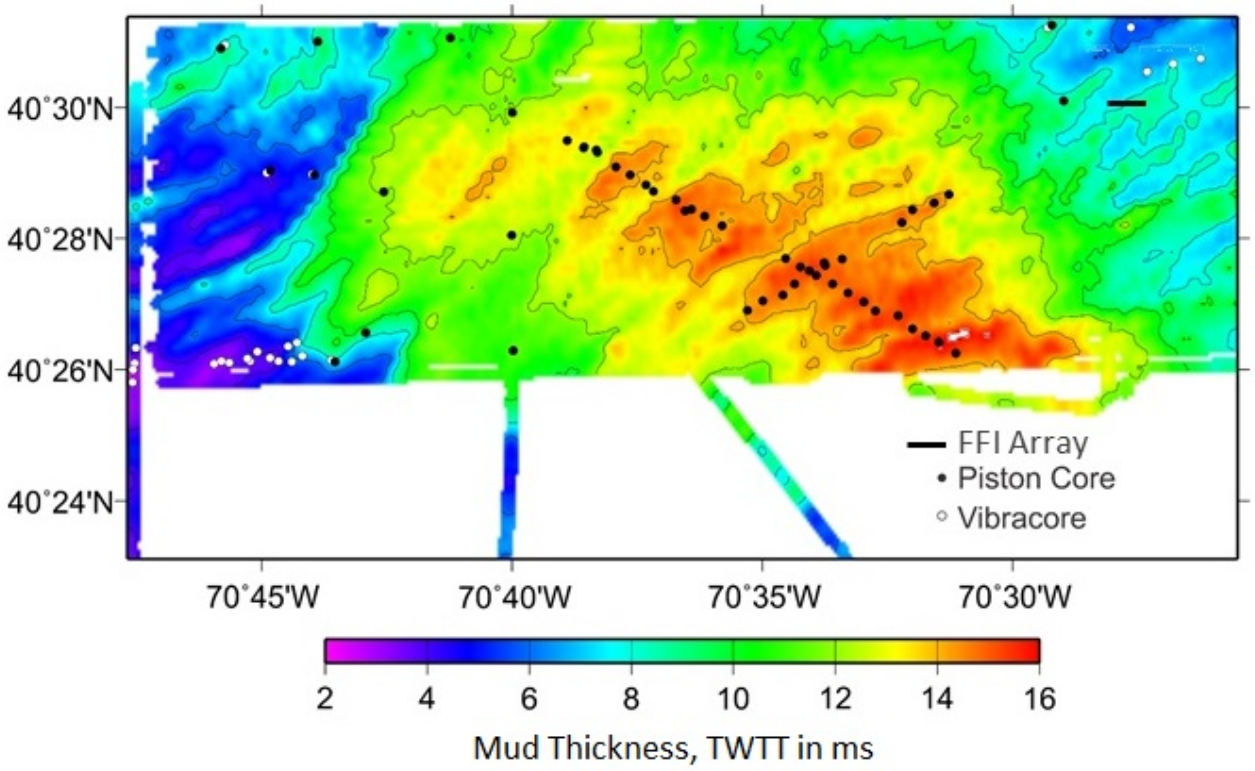

Fig. 1. SBCEX17 area on the New England Mud Patch with map indicating the two-way travel time (TWTT) to a reflection horizon from a subbottom profiling sonar interpreted as the base of an upper mud sediment layer [14]. Symbols indicate positions of piston cores (black dots) and vibracores (white dots), and the approximate location of the FFI array (black line).

Fig. 1 shows a map of the SBCEX17 area indicating the two-way travel time (TWTT) to a reflection horizon from the subbottom profile which is interpreted as the base of an upper mud sediment layer [14]. The TWTT is approximately 4–10 ms in the NE part of the experiment area; at the location of the FFI array the TWTT is 6–8 ms. These TWTTs correspond approximately to a mud layer thickness of 3–7.5 m in the NE part of the area, and to 4.5–6 m at the FFI array location (assuming an average sediment sound speed of 1500 m/s).

Core measurements in the vicinity of the array include two piston cores and five vibracores [15]. The piston core measurement closest to the FFI array is denoted 43PC and is located approximately 1.83 km to the west of the array midpoint. Piston core 41PC is approximately 3.28 km northwest of the array. Fig. 2 shows results from core-logger measurements on 43PC and 41 PC in terms of sediment sound speed and density [16]. The 43PC core measurements to 2 m depth indicate a low-speed (1457–1535

Dette er en postprint-versjon/This is a postprint version.
DOI til publisert versjon/DOI to published version: 10.1109/JOE.2019.2908026

m/s, median 1486 m/s) and medium-density (1.64–1.87 g/cm³, median 1.74 g/cm³) sediment, consistent with properties of fine-grained sediment [15]. The core measurements at 4–6 m depth indicate a higher-speed (1628–1850 m/s, median 1745 m/s) and higher-density (2.01–2.25 g/cm³, median 2.11 g/cm³) sediment, consistent with coarse-grained sediments (e.g., sand). Measurements on piston core 41PC also indicate a low-speed (1466–1534 m/s, median 1486 m/s) and medium-density (1.53–1.77 g/cm³, median 1.69 g/cm³) sediment to 2 m depth (the core extended to less than 4 m depth).

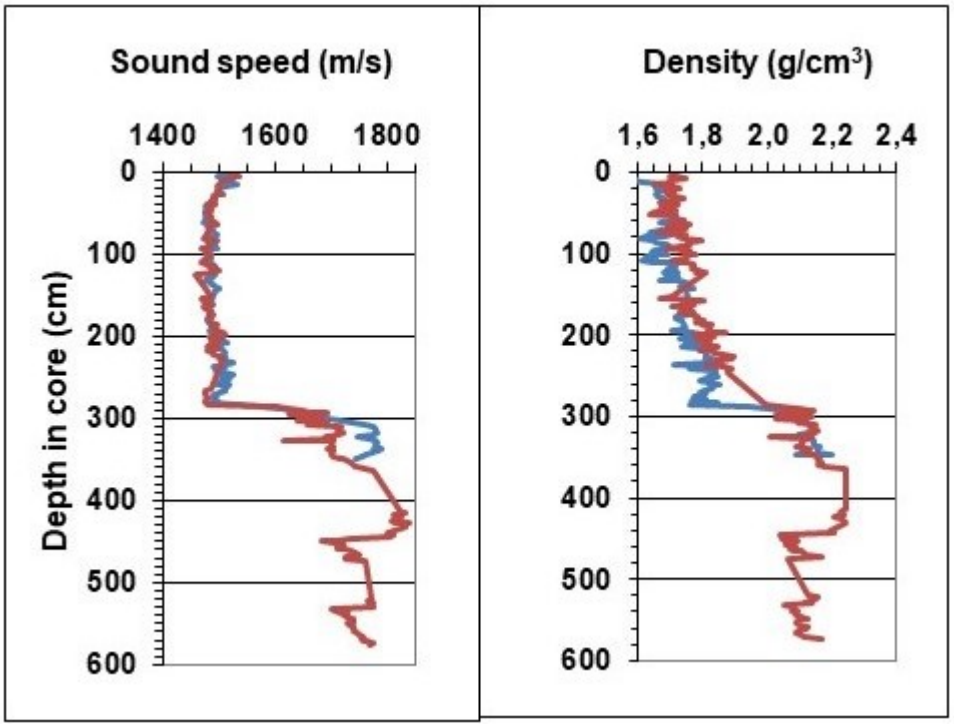

Fig. 2. Sediment core analysis results for piston cores 43PC (red) and 41PC (blue) [16].

Fig. 3 shows an interpreted seismic section based on data from the subbottom profiling sonar survey [14]. The section in Fig. 3 extends from approximately 8 km west of the FFI array (left side of Fig. 3) to 1 km east of the FFI array (right side of Fig. 3), within 300 m south of the array. The dashed yellow line in Fig. 3 indicates the western limit of the area over which the acoustic data considered in this paper were collected. Indicated is a mud unit (between the seafloor/mudbase reflectors) with a number of internal reflectors above a thin layer (between the mudbase/sandbase reflectors) over a base. The reflectors that define layer interfaces are reasonably parallel and horizontal over the area where the acoustic data were collected and, hence, the assumption that the seabed can be treated as range

DOI til publisert versjon/DOI to published version: 10.1109/JOE.2019.2908026

independent seems reasonable.

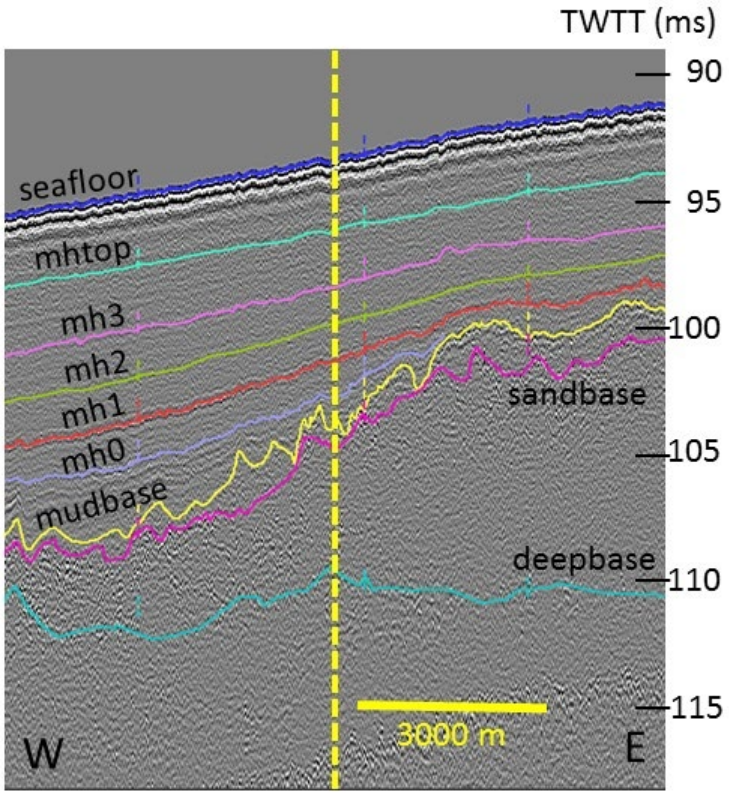

Fig. 3. Interpreted seismic section west-east in the SBCEX17 experiment area [14]. The section extends from approximately 8 km west of to 1 km east of the FFI array, within 300 m south of the array. The dotted yellow line indicates the western limit of the area where the acoustic data analyzed in this paper were collected.

The FFI array was located within approximately 2 nmi (3.7 km) from the southern limit of the shipping lane leading to the Port of New York and New Jersey. An average of three large commercial ships passed the array each day it was deployed (March 10 to April 7). Selected here for analysis are acoustic data recorded due to a large container ship passage that occurred on March 13. Fig. 4 shows the ship track (the portion selected for analysis) and the position of the FFI array. The ship approached from the east (at the southern limit of the shipping lane) then turned to enter the experiment area and passed with a closest point of approach (CPA) at 070150UTC at range 2.1 km from the array.

Dette er en postprint-versjon/This is a postprint version.
DOI til publisert versjon/DOI to published version: 10.1109/JOE.2019.2908026

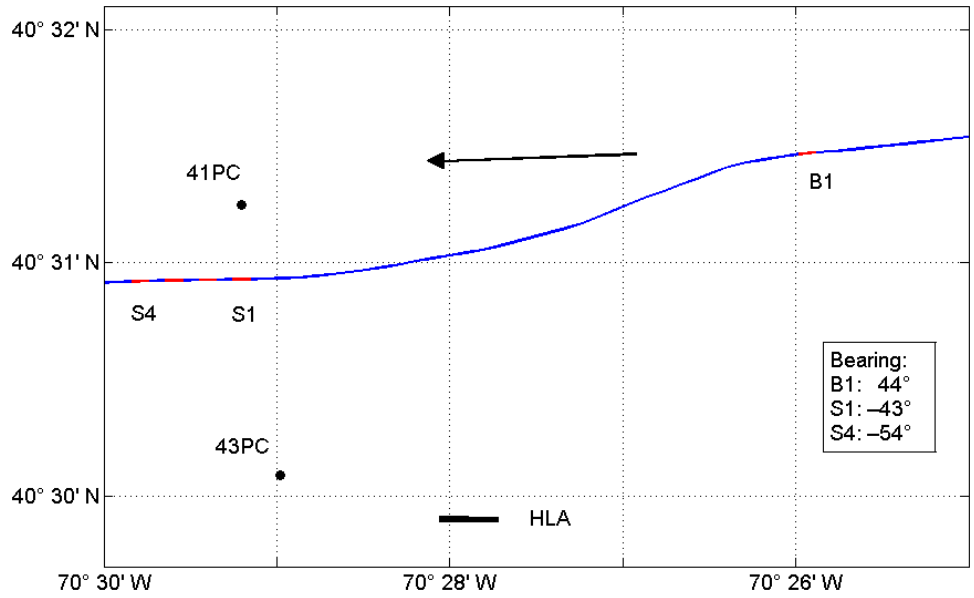

Fig. 4. Track of the container ship M/V *Ever Living* (blue line), locations of the FFI array (blue line), data segments used for inversions (red), and of piston cores 43PC and 41PC (black dots). The arrow indicates the ship direction of travel.

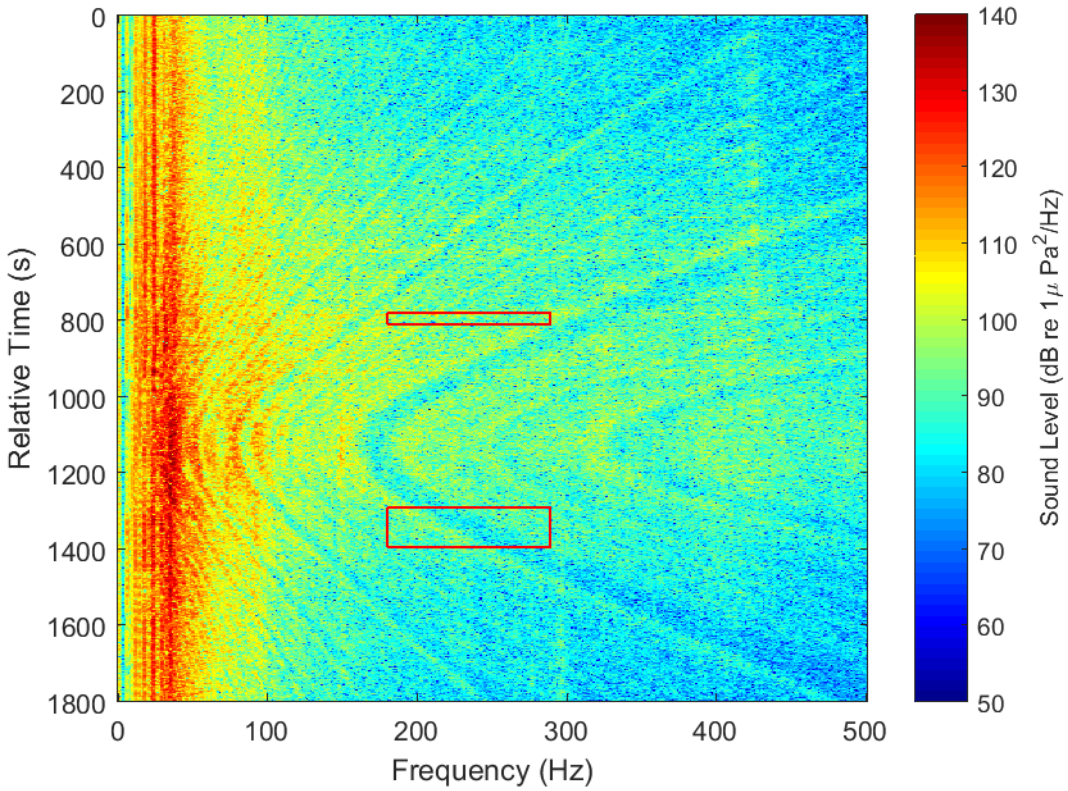

Fig. 5. Spectrogram from time period of passage of container ship M/V *Ever Living*, acoustic data recorded on hydrophone 13 of the FFI horizontal array on the seabed. Red boxes denote data selected for inversions.

Dette er en postprint-versjon/This is a postprint version.
DOI til publisert versjon/DOI to published version: 10.1109/JOE.2019.2908026

The ship, M/V *Ever Living* (IMO 9629031), has a length of 335 m and gross tonnage 99,946 T; the average ship speed during the passage was 18 kts (9.25 m/s). Table I contains further technical information on the ship.

Fig. 5 shows the spectrogram from a single hydrophone (number 13) recording of the container ship passage. The spectrogram shows a typical "bathtub" interference pattern, shifting with time as the ship-hydrophone range changes. Distinct frequency lines (tonal frequencies) within the frequency band 6–150 Hz are related to propeller and machinery generated noise [17], [18] and can be seen over the extent of the ship passage. Broadband radiated ship noise is seen over the entire frequency band to 500 Hz.

Acoustic array data, sampled at 5 kHz, were processed with 4096 point FFTs (1.22 Hz frequency resolution). Selected for inversions were data at seven frequency bins centered on 180, 190, 200, 210, 220, 280, and 290 Hz, representing broadband radiated ship noise (avoiding tonal frequencies). Cross-spectral density matrices (CSDMs) for 8 s data segments were formed using 18 consecutive snapshots, each of duration 0.82 s, applying 50%-overlapped Hamming windows. The ship traversed approximately 7.6 m over the duration of a snapshot and 72 m over the duration of a segment. Data segments were formed starting at each 15 s interval from 065600UTC to 070600UTC (41 segments over 10 minutes). Data were processed separately for bow (pre-CPA) and stern (post-CPA) ship aspects.

A nominal ship track was derived from ship Automatic Identification System (AIS) data obtained from the United States Coast Guard Navigation Center Nationwide AIS database. AIS message data (latitude/longitude geographic positions) were interpolated to 15 s time resolution. Data segment range relative to the array center and bearing relative to array broadside (positive clockwise re N) were 4.1 km and 44° for bow aspect data (segment B1), and 2.61−3.22 km and −43° to −54° for stern aspect data (segments S1–S4) considered in the following. The ship aspect angle (azimuthal angle, clockwise re bow) was 319° for bow aspect data and 228° (segment S1) to 218° (segment S4) for stern aspect data. Table II lists information on the data segments considered in the following. Data segments closer in range (to CPA) are also closer to the array broadside direction; the geoacoustic information content of

DOI til publisert versjon/DOI to published version: 10.1109/JOE.2019.2908026

HLA acoustic data in matched-field inversion is generally lower for broadside sources (due to reduced longitudinal array aperture) and, hence, were not selected for analysis here.

The fluid seabed model allows for 1–6 sediment interfaces over a halfspace. (The upper limit of 6 interfaces was set to maintain numerical stability of the normal-mode propagation model used in the inversions, and is expected to be sufficient for the amount of structure resolvable by ship-noise data.) In the geoacoustic model, the interval between two sediment interfaces defines a homogeneous sediment layer and is here described by sound speed (c), density (ρ) and attenuation (α) parameters. Table III (left columns) lists the model geoacoustic parameters and prior bounds. A measured sound speed profile in water was used, collected from the R/V *Neil Armstrong* on March 12 at 234200UTC at a position approximately 8.5 km southwest of the array. The water column was almost isospeed, with the sound speed increasing linearly with depth from 1468.1 m/s at the top to 1469.0 m/s at the bottom of the water column. The sea conditions were moderate (WMO sea state code 3–4, wind speed 13–18 kts) during the period of acoustic data collection on March 13.

Uncertain geometric parameters include water depth (D), source depth (z), and source range (r_j) and bearing (θ_j) for each data segment j. Water depths were inferred from a bathymetric model based on data collected with the subbottom profiler, by converting from measured TWTT to the seafloor reflector using an average water sound speed of 1490 m/s (from the pilot survey). From the bathymetric model, water depths along radials extending to a range of 4 km in directions NE, N, and NW from the array are within 66.4–68.7 m, with a depth of 68.7 m at the array site (NE and N: 66.4–68.7 m, NW: 68.0–68.7 m). In the inversions, wide uniform prior bounds for water depth of 64.8–70.8 m were used, within the limits of the bathymetric model, also allowing for tidal elevations at the time of acoustic data collection (assumed to be within ±0.8 m). Note that the model water depth here (in range-independent inversions) represents an *effective* water depth for an equivalent flat bathymetry approximation to a weakly range-dependent bathymetry [19]. This approximation seems justified for the present environment (the slope between the array position and the ship track is less than 0.04°) and has been used in a number of previous matched-field inversion studies [4], [12].

DOI til publisert versjon/DOI to published version: 10.1109/JOE.2019.2908026

The broadband radiated ship noise over the band 180−290 Hz is represented as an acoustic point source in the inversions. Broadband ship noise at these frequencies is predominately due to the rapid formation and collapse of bubbles (cavities) induced by the ship's propeller at or above cavitation speed [17], and is generated in a small region near the upper tip of the propeller blades [20]. Given the small dimensions of this region (the propeller size is less than the ship's draft of 14.2 m), at the relatively low frequencies and long ranges considered here, a point source model is appropriate.

Gray and Greeley [20] introduced a source depth model for propeller-induced noise; using the AIS-reported draft of 11.8 m and assuming a propeller diameter of 7.1 m (one-half of the ship's maximum draft), this model yields a source depth of 5.8 m. Wales and Heitmeyer [21] suggested a depth-distributed model centered near this depth. Without further known details of *M/V Ever Living*, wide uniform prior bounds of 3–12 m on source depth were adopted in all inversions. For multiple-segment inversions, the source depth is also treated as an unknown parameter but is assumed to be constant for all segments, i.e., assumed to not change between segments.

The nominal source-to-array range was computed for each data segment from the ship AIS position (at the center time of the data segment) to the array center, then reduced/increased by an assumed AIS position to ship stern separation of 50 m for stern/bow aspects, respectively. The nominal source bearing (relative to array broadside) was computed from the array center to the ship position (computed as described above). For source range, a ±0.125 km uniform prior bound is centered on the nominal source-to-array range. For source bearing, a ±6° uniform prior bound is centered on the nominal ship bearing.

The number of uncertain model parameters then is $4k$ +3 geoacoustic parameters (with k the number of sediment interfaces), and $2J$ +2 geometric parameters (with J the number of data segments). Nominal hydrophone locations along the array were used based on the known array element separations and assumed straight-line array geometry. The array orientation (0.2° with respect to east-west) was derived from acoustic positioning (via triangulation) of the array end elements. The array element depths were taken to be 0.05 m above the water-sediment interface. To reduce computational effort, a 20-element

subsection of the full 64-element array (elements 3–22) was used in the present study. The elements of this subsection were unevenly spaced (14–72 m), with overall length 480 m. The ORCA normal-mode forward model [22] was used to compute replica (predicted) acoustic fields in the inversion. Replica fields were computed at the processing frequencies; waveguide Doppler effects due to source motion [23] are assumed to be minor, and are neglected.

III. THEORY

This section provides an overview of Bayesian trans-D inversion. More complete treatments of Bayesian methods and/or Markov-chain Monte Carlo methods, some with applications in geoacoustic inversion, are given in [11]–[13], [24]–[29]. In particular, the algorithm implementation used in this paper is based primarily on the development in Ref. [13], which is summarized here.

A. Trans-D Bayesian inversion

Let K be a countable set, indexed by k, specifying choices of model parameterization (e.g., number of seabed layer interfaces) with the corresponding sets of M_k free parameters denoted $\mathbf{m}_k$, and let $\mathbf{d}$ represent observed data. Bayes' theorem for a hierarchical model including hyper-parameter k can be written [24]

$$P(k,\mathbf{m}_k \mid \mathbf{d}) = \frac{P(k)P(\mathbf{m}_k \mid k)P(\mathbf{d} \mid k,\mathbf{m}_k)}{\sum_{k'\in\kappa}\int_{\mathcal{M}_{k'}} P(k')P(\mathbf{m}'_{k'} \mid k')P(\mathbf{d} \mid k',\mathbf{m}'_{k'})d\mathbf{m}'_{k'}}, \tag{1}$$

where $\mathcal{M}_k$ represents the M_k-dimensional parameter space associated with index k. In (1), $P(k)P(\mathbf{m}_k|k)$ is the prior probability of the state (k, $\mathbf{m}_k$), and $P(\mathbf{d}|k, \mathbf{m}_k)$ is the conditional probability of $\mathbf{d}$ given (k, $\mathbf{m}_k$), which is interpreted as the likelihood of (k, $\mathbf{m}_k$), denoted $L(k, \mathbf{m}_k)$. The posterior probability density (PPD) $P(k, \mathbf{m}_k|\mathbf{d})$ is defined over the trans-D parameter space which represents the union of all fixed-D subspaces specified by κ. The denominator (normalization) on the right side of (1) represents the total

DOI til publisert versjon/DOI to published version: 10.1109/JOE.2019.2908026

Bayesian evidence of the set of possible models.

The PPD in (1) can be sampled by constructing a Markov chain that transitions between models with differing numbers of parameters (dimensions) while satisfying reversibility (i.e., the probability of stepping from one model to another is the same as the probability of the reverse step). This can be accomplished by accepting a new state $(k', \mathbf{m}'_{k'})$, given a current state $(k, \mathbf{m}_k)$, with probability given by the Metropolis-Hastings-Green criterion [24]

$$A(k', \mathbf{m}'_{k'} \mid k, \mathbf{m}_k) = \min\left[1, \frac{Q(k, \mathbf{m}_k \mid k', \mathbf{m}'_{k'})}{Q(k', \mathbf{m}'_{k'} \mid k, \mathbf{m}_k)} \frac{P(k')P(\mathbf{m}'_{k'} \mid k')}{P(k)P(\mathbf{m}_k \mid k)} \frac{L(k', \mathbf{m}'_{k'})}{L(k, \mathbf{m}_k)} |\mathbf{J}|\right]. \quad (2)$$

In (2), $Q(k', \mathbf{m}'_{k'} \mid k, \mathbf{m}_k)$ is the proposal probability density of proposing a new state $(k', \mathbf{m}'_{k'})$ given the current state $(k, \mathbf{m}_k)$, and $|\mathbf{J}|$ is the determinant of the Jacobian matrix for the coordinate transformation between parameter sub-spaces. Trans-D sampling according to (2) is carried out using reversible-jump Markov-chain Monte Carlo (rjMCMC). The most common form of rjMCMC in geophysical inversion adds and deletes layers (referred to as birth and death steps, respectively) in such a manner that $|\mathbf{J}| = 1$. The requirements are that the interface depths are independent from layer parameters (i.e., partition modeling), and that only the parameters added/deleted in birth/death steps are changed, with proposed parameters in a birth step depending (at most) on the parameters at that depth in the current state. In addition to birth and death steps, rjMCMC carries out perturbation steps where parameters of the current model are perturbed randomly without changing model dimension. For the case of uniform bounded priors for geoacoustic parameters and hyperparameter k, a uniform prior for interface depths represented by a Dirichlet prior for the depth partition [29], a symmetric proposal density for perturbation steps, and the parameters of new layers in birth steps drawn from the prior, it can be shown that the acceptance criterion for all steps reduces to the likelihood ratio [13]

$$A(k', \mathbf{m}'_{k'} \mid k, \mathbf{m}_k) = \min\left[1, \frac{L(k', \mathbf{m}'_{k'})}{L(k, \mathbf{m}_k)}\right]. \quad (3)$$

Further, several studies have shown that proposing birth parameters from the prior results in a more-

DOI til publisert versjon/DOI to published version: 10.1109/JOE.2019.2908026

efficient algorithm than applying a proposal density focused near the current values [13]. Efficient sampling of the PPD depends on effective proposal schemes within the rjMCMC algorithm. In this paper, the proposal density is based on sampling in a principal-component parameter space [13], rotated to remove inter-parameter correlations, and on parallel tempering [12], [13], [31]−[33], which carries out sampling using a sequence of interacting Markov chains which consider progressively relaxed versions of the likelihood function.

B. Likelihood function

The data considered in this paper consist of complex (frequency-domain) acoustic fields measured at an N-sensor array and F frequencies corresponding to J distinct segments of the recorded acoustic pressure time series, with each time segment divided into S sub-segments referred to as snapshots, i.e., $\mathbf{d} = \{\mathbf{d}_{fjs},\ f=1,F;\ j=1,J;\ s=1,S\}$. The source-receiver range is considered to be fixed over the S snapshots comprising each data segment, but range varies between segments. The source spectrum is considered unknown over frequency and time with parameters $\mathbf{A}=\{A_{fjs}\}$ and $\boldsymbol{\theta}=\{\theta_{fjs}\}$ representing unknown amplitudes and phases, respectively. The data errors are assumed to be uncorrelated, circularly-symmetric complex Gaussian-distributed random variables, with unknown variances $\boldsymbol{\nu}$ which depend on frequency and data segment but are considered constant over snapshots (within a segment) and over hydrophones, i.e., $\mathbf{v}=\{\nu_{fj}\}$. In this case, the likelihood function is given by [4]:

$$L(\mathbf{m},\mathbf{A},\boldsymbol{\theta},\mathbf{v}) = \prod_{f=1}^{F}\prod_{j=1}^{J}\prod_{s=1}^{S}\frac{1}{(\pi\nu_{fj})^{N}}\exp\left[-\left|\mathbf{d}_{fjs} - A_{fjs}e^{i\theta_{fjs}}\mathbf{d}_{fj}(\mathbf{m})\right|^{2}/\nu_{fj}\right], \tag{4}$$

where $\mathbf{d}(\mathbf{m})$ represents modeled (replica) data computed for model $\mathbf{m}$ (the trans-D nature of the inversion is not important here, so the notation specifying the number of interfaces is omitted). The explicit dependence on source spectral parameters and error variances can be removed by setting $\partial L/\partial A_{fjs} = \partial L/\partial \theta_{fjs} = \partial L/\partial \nu_{fj} = 0$ to obtain maximum-likelihood expressions which are then substituted back into (4), leading to misfit (negative log-likelihood) function:

$$E = SN\sum_{f=1}^{F}\sum_{j=1}^{J}\log_e\left\{\mathrm{Tr}\left\{\mathbf{C}_{fj}\right\}-\frac{\sum_{s=1}^{S}\left|\mathbf{d}_{fjs}^{\mathrm{H}}\mathbf{d}_{fj}(\mathbf{m})\right|^2}{S\left|\mathbf{d}_{fj}(\mathbf{m})\right|^2}\right\}, \tag{5}$$

where

$$\mathbf{C}_{fj}=\frac{1}{S}\sum_{s=1}^{S}\mathbf{d}_{fjs}\mathbf{d}_{fjs}^{\mathrm{H}} \tag{6}$$

is the data CSDM for the f-th frequency and j-th time segment defined by the ensemble average over the S snapshots. Here, Tr{•} and $^{\mathrm{H}}$ represent, respectively, the matrix trace and conjugate (Hermitian) transpose. Explicitly sampling this misfit function over model parameters **m** implicitly samples over the corresponding maximum-likelihood estimates for source spectrum and variances. Note that in the misfit (5), the measured complex acoustic field over the array for each snapshot, data segment, and frequency is correlated with the replica field corresponding to that segment and frequency. Hence, it is the spatial variation of the complex field (amplitude and phase) over the array aperture that provides coherent information content. These correlations are summed incoherently over snapshot, data segment, and frequency.

IV. RESULTS

Results from inversions of ship-noise data are presented here for three cases: a post-CPA data segment at range 2.80 km at stern ship aspect, a pre-CPA data segment at range 4.07 km at bow ship aspect, and multiple post-CPA data segments over ranges 2.61–3.22 km at stern ship aspect (each segment comprises 8 s of data).

A. Stern aspect data

Fig. 6 shows the marginal posterior probability profiles for interface depth, sound speed, density, and

DOI til publisert versjon/DOI to published version: 10.1109/JOE.2019.2908026

attenuation (to 30 m depth below the water-sediment interface) from the inversions of stern-aspect data at 2.80 km range. The marginal profiles for sound speed, density, and attenuation are normalized individually at each depth, with warm (red) colors indicating high probability and cool (blue) colors representing low probability (white is zero probability). For all parameters, the plot bounds correspond to the prior bounds. The interface marginal profile (left panel) indicates high probability for an interface at 3–7 m depth (with a peak at ~5.5 m), and a relatively low probability of additional interfaces approximately uniformly distributed to the maximum depth. The sediment sound speed profile indicates an upper homogeneous low-speed layer (e.g., mean and mean-deviation sound speed 1526±33 m/s at 0 m depth), a transition layer at about 3–7 m depth (sound speed 1581±53 m/s at 5 m) with sound speed increasing over the depth interval, and a halfspace of higher sound speed (e.g., 1678±53 m/s at 10 m). (There is also a possible indication of a higher-speed layer, or at least higher uncertainty in sound speed, at greater depths; however, the interface marginal profile does not resolve an interface depth.) Density is generally poorly constrained by the data, although relatively high densities (1.98±0.20 g/cm^3 at 0 m) are indicated in the upper part of the seabed. The relatively poorly constrained density values in the upper part of the seabed likely result from the inability of short-range acoustic data to resolve an inherent sound-speed/density ambiguity, often observed in matched-field inversions. Attenuation also is generally poorly constrained by the data. Table III provides the prior bounds and the mean and mean deviation values for the seabed parameters, at selected depths of 0 m, 5 m, and 10 m.

DOI til publisert versjon/DOI to published version: 10.1109/JOE.2019.2908026

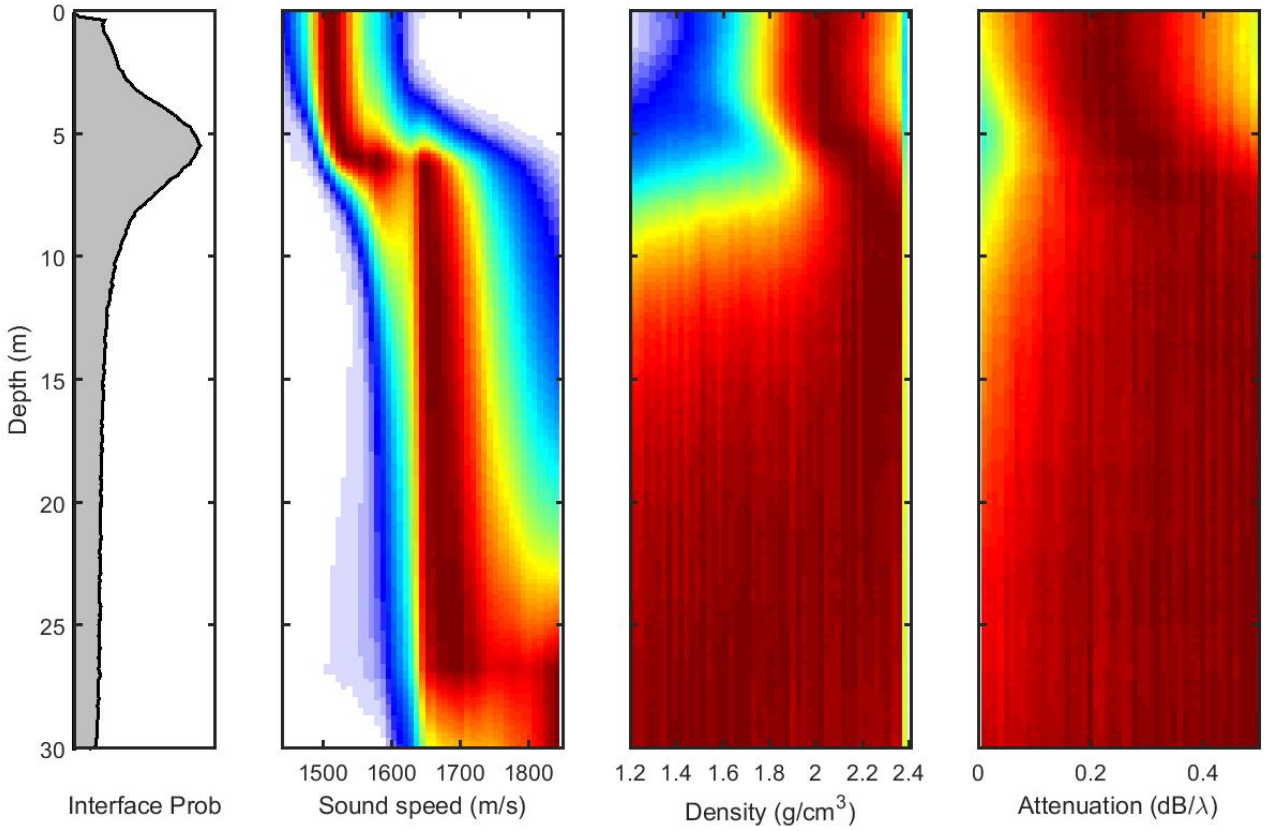

Fig. 6. Marginal posterior probability profiles for interface depth, sound speed, density, and attenuation. Data segment range 2.80 km, stern aspect.

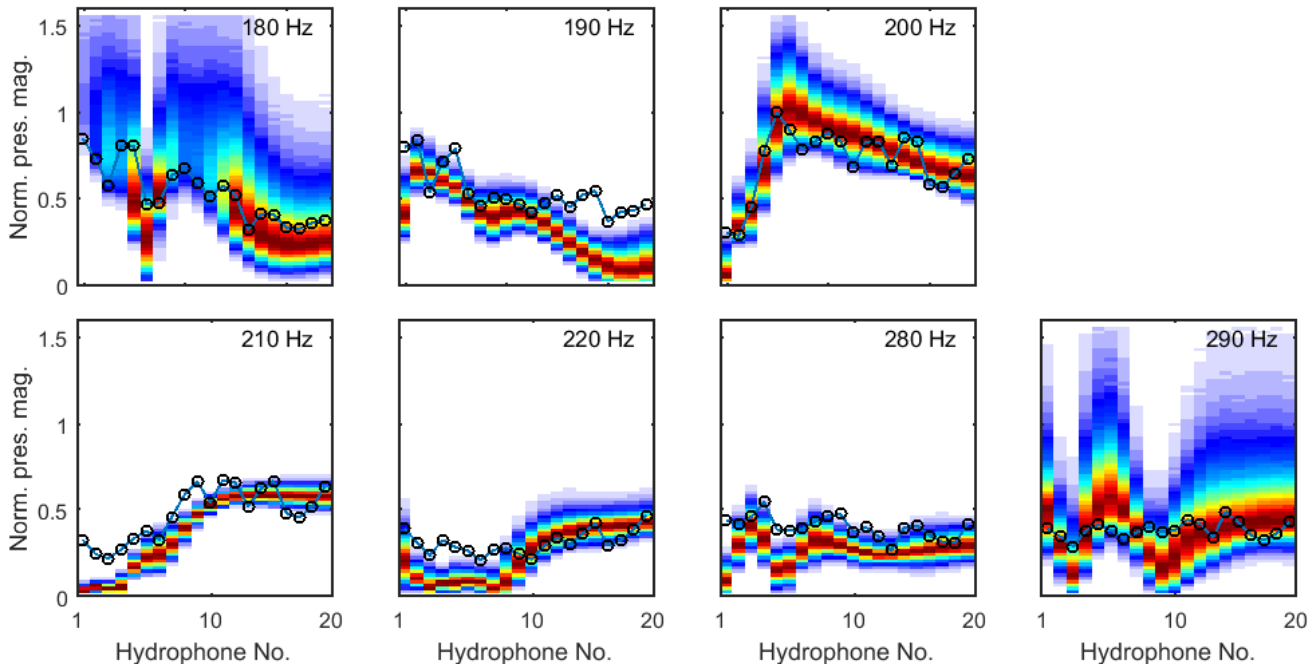

Fig. 7. Measured data (solid line and open circles) and predicted data probability densities (color) in terms of normalized pressure magnitude as a function of hydrophone number and frequency. Data segment range 2.80 km, stern aspect.

Dette er en postprint-versjon/This is a postprint version.
DOI til publisert versjon/DOI to published version: 10.1109/JOE.2019.2908026

Fig. 7 shows the measured and predicted acoustic data in terms of (snapshot-averaged) pressure magnitude. The predicted data represent probability densities computed from the PPD samples collected in the inversion. Each panel represents a frequency included in the inversion. The horizontal axis is hydrophone number (for display purposes not to length scale). Overall, the predicted data fit the measured data reasonably well, with largest uncertainties at the lowest and highest frequencies. Fig. 8 shows marginal probability densities of the estimated data-error standard deviations at each frequency (normalized by the maximum measured pressure magnitude). The standard deviations are all narrowly distributed around mean values within 0.17–0.30, indicating significant uncertainties in the ship-noise data, with highest standard deviations at the three lowest frequencies.

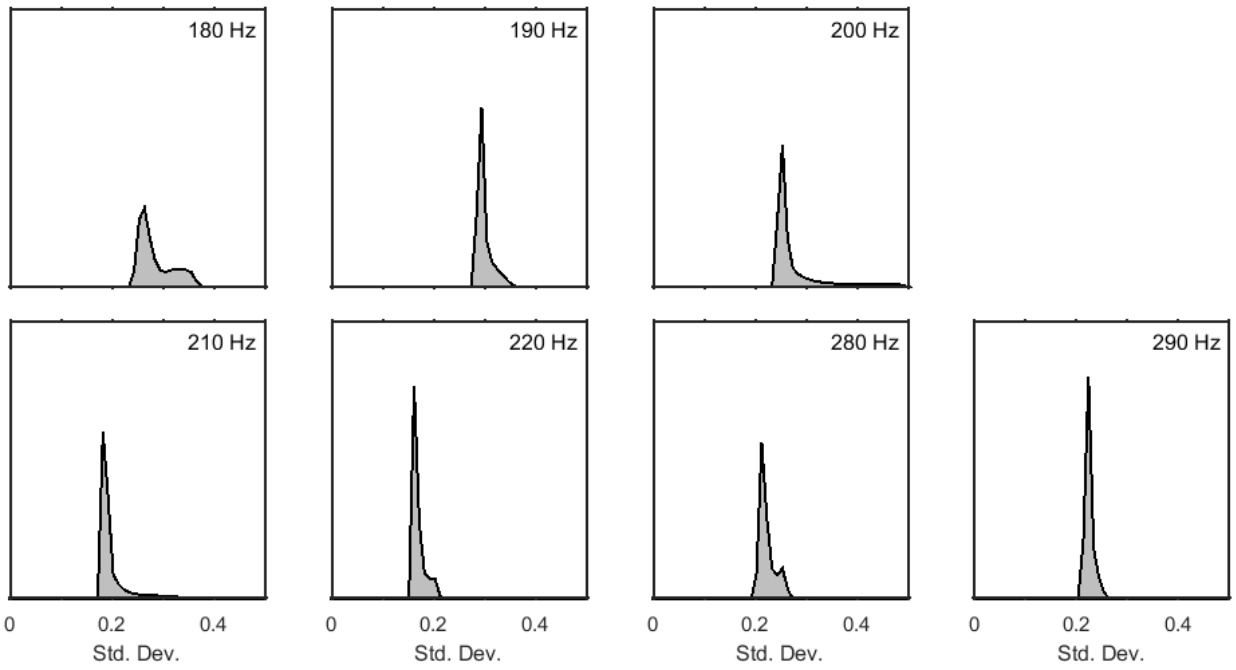

Fig. 8. Marginal probability densities of estimated data-error standard deviations. At each frequency, the standard deviation is normalized by the maximum measured pressure magnitude.

The variability in data-error standard deviations over the hydrophone array (computed from residuals) at each frequency was found to be relatively small. In particular, the ratio of the standard deviation to the mean of the data-error standard deviations was about 0.2 at each frequency (i.e., about 20% variability), consistent with the assumption of uniform variances over hydrophones. The assumptions on the data error statistics (Sec. III.B) were checked by performing *a posteriori* tests on standardized

Dette er en postprint-versjon/This is a postprint version.
DOI til publisert versjon/DOI to published version: 10.1109/JOE.2019.2908026

residuals [34], here at each frequency for each data snapshot for a random selection of 1000 models from the PPD. The Lilliefors test provided no evidence against the hypothesis of Gaussian-distributed errors at the 0.05 significance level in more than 85% of tests at six of seven frequencies. The runs test provided no evidence against spatial randomness (i.e., serial correlations between elements of the HLA) at the 0.05 significance level in more than 94% of tests at all frequencies.

Fig. 9 (upper) shows the misfit (5) as a function of rjMCMC step and a distribution of the misfit values (a burn-in phase of 3000 samples was discarded). The misfit values are randomly distributed with no apparent trend in values, indicating stationary chain sampling. Stationary chain sampling was similarly indicated all of the inversion cases considered in this paper. Sampling convergence was checked by comparing the marginal probability profiles from the first and second halves of the total sample. In the inversion cases considered in this paper the results were essentially identical, indicating that the inversion results had ceased to change and were considered to have converged. Fig. 9 (lower) shows the number of interfaces k as a function of rjMCMC step and as a marginal probability distribution. The figure shows that stationary sampling over k has been achieved. The marginal probability for the number of interfaces has a peak at 1 and decreases as k increases from 1–6. Similar probability distributions with a peak at 1 interface were obtained in all the inversion cases considered in this paper.

Dette er en postprint-versjon/This is a postprint version.
DOI til publisert versjon/DOI to published version: 10.1109/JOE.2019.2908026

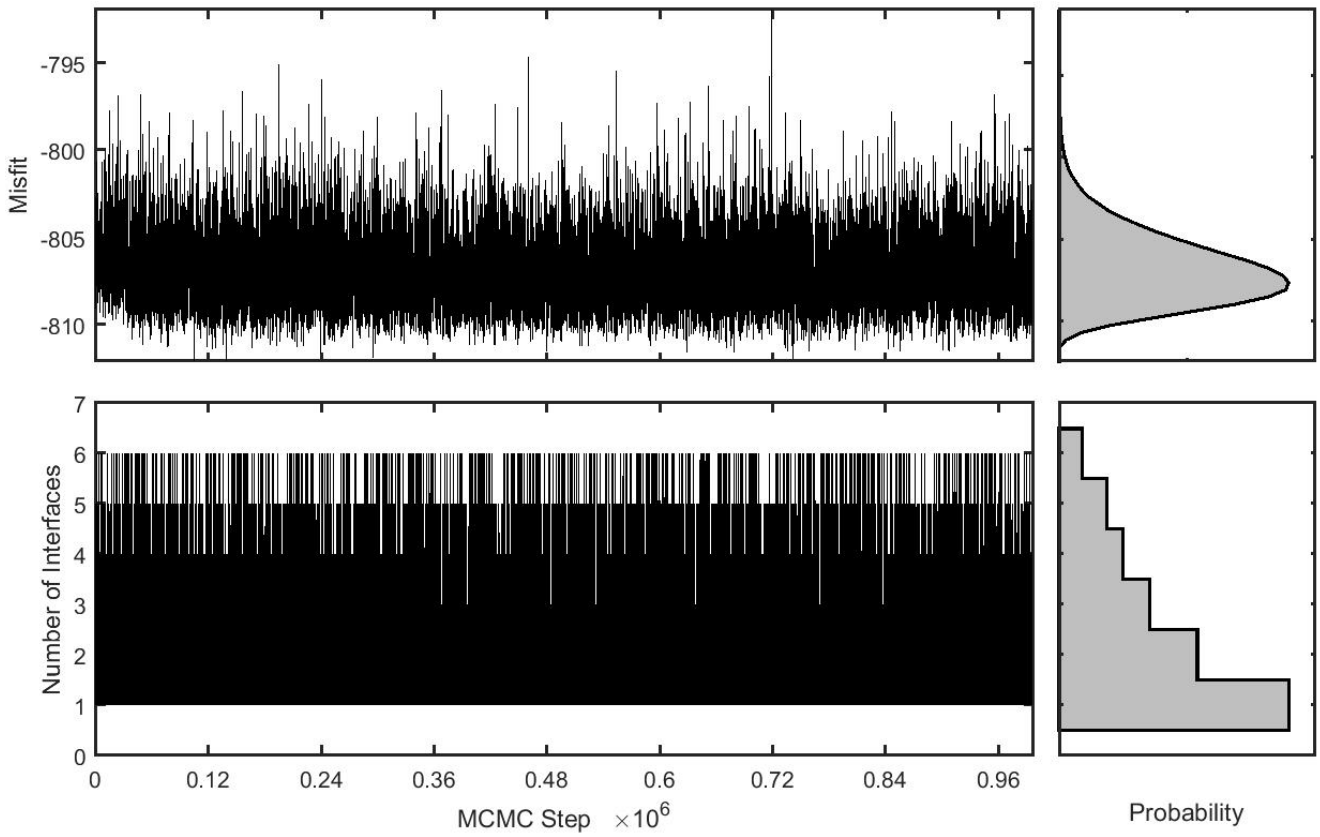

Fig. 9. (Upper) Misfit as a function of rjMCMC step and misfit marginal density; (Lower) number of interfaces as a function of rjMCMC step and marginal distribution. Data segment range 2.80 km, stern aspect.

B. Bow aspect data

In this section, inversion of data from the ship at bow aspect is presented for a range of 4.07 km. Fig. 10 shows marginal probability profiles. The inversion indicates a two-layer seabed structure, with a low-speed upper layer (1511±34 m/s at 0 m depth) to approximately 3–7 m depth (interface probability peak at 4.6 m) over a higher-speed deeper layer (1705±58 m/s at 10 m). The density is high but with large uncertainty in the upper layer (1.80±0.21 g/cm³ at 0 m) and unconstrained in the lower layer. The attenuation is essentially unconstrained, although low probability of low attenuation is indicated in the upper part of the seabed.

Dette er en postprint-versjon/This is a postprint version.
DOI til publisert versjon/DOI to published version: 10.1109/JOE.2019.2908026

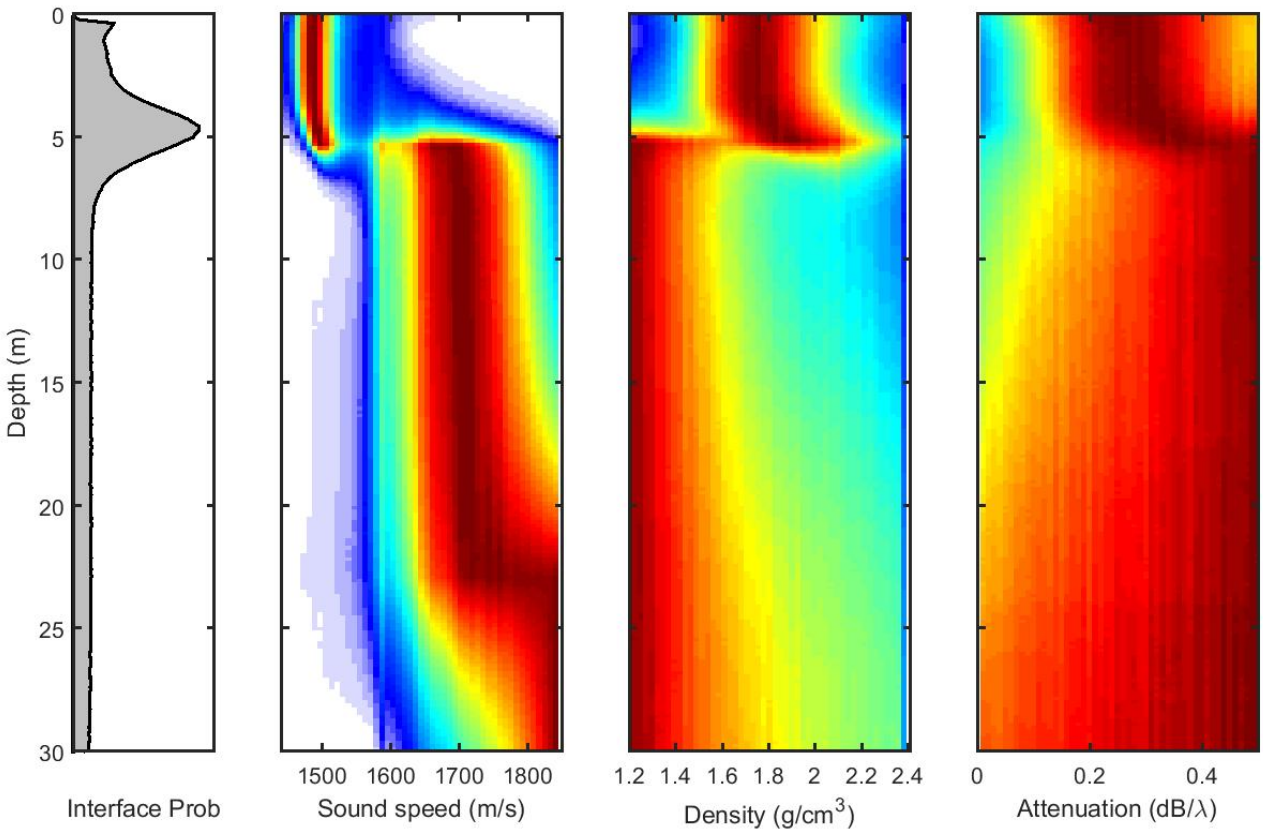

Fig. 10. Marginal posterior probability profiles for interface depth, sound speed, density, and attenuation. Data segment range 4.07 km, bow aspect.

The inversion results are reasonably consistent with those obtained from the inversions of stern data (Sec. IV.A): both indicate a low-speed upper sediment region over higher-speed sediments. The interface depth (indicated at 3–7 m depth) is consistent between the inversions. The marginal probability profiles for sound speed have considerable overlap between the stern-aspect and bow-aspect data inversions such that the two values cannot be distinguished clearly given uncertainties. The slightly different distributions may be due to different data information content between the bow/stern aspect data segments resulting from: (1) differences in radiated ship noise level between bow/stern aspect, and (2) increased attenuation of higher-order modes with the longer range bow-aspect data which can reduce the resolution of seabed parameters (due to loss of information from the short vertical wavelengths of these modes) [4]. Ship radiated noise levels are often reported lower at bow than stern ship aspect [17], however, there is significant radiated noise from bow aspect of the ship considered here (Fig. 5).

Dette er en postprint-versjon/This is a postprint version.
DOI til publisert versjon/DOI to published version: 10.1109/JOE.2019.2908026

C. Multiple data segments

This section presents results for simultaneous inversion of 4 data segments (at stern aspect) over a range interval of 2.61–3.22 km. (The data segments, including the segment considered in Sec. IV.A, were of length 8 s each, separated in time by 22 s, for a total time span of 98 s.) Multiple data segments may increase data information content for low signal-to-noise ratio (SNR) data, at the expense of more geometric parameters and longer computation time for data prediction (roughly by a factor J over single-segment inversions) per sampled model. Note that with the misfit function (5), source amplitude is considered unknown from segment to segment and hence can account for variation due to ship source directionality.

Fig. 11 shows marginal probability profiles. The inversion indicates a distinct two-layer seabed structure, with a low-speed upper layer (1508±22 m/s at 0 m) to approximately 3–7 m depth (interface probability peak at 5.0 m) over a high-speed halfspace (sound speed 1678±37 m/s at 10 m). The density is estimated as 1.89±0.16 g/cm³ in the upper part of the seabed. There is large uncertainty in density in the lower part of the seabed. Attenuation is indicated low in the upper part of the seabed (0.16±0.09 dB/λ at 0 m, acoustic wavelength λ) although the uncertainty may not be representative since the posterior distribution is cut off at its lower prior bound, and unconstrained in the lower part. The solid lines in Fig. 11 show the measured values of sediment sound speed and density from piston core 43PC (discussed further in Sec. IV.E).

Some observations can be made by comparing the multiple-segment stern data inversion results with the single-segment stern data inversion (Sec. IV.A) results: (1) sound speed: the marginal probability profile widths are narrower (smaller uncertainties) from the multiple-segment inversion (see Table III); (2) transition layer: details of the sound speed in the transition layer at 3–7 m depth suggested in the single-segment inversion (Fig. 6) is not as distinct in the multiple-segment inversion (Fig. 11).

Dette er en postprint-versjon/This is a postprint version.
DOI til publisert versjon/DOI to published version: 10.1109/JOE.2019.2908026

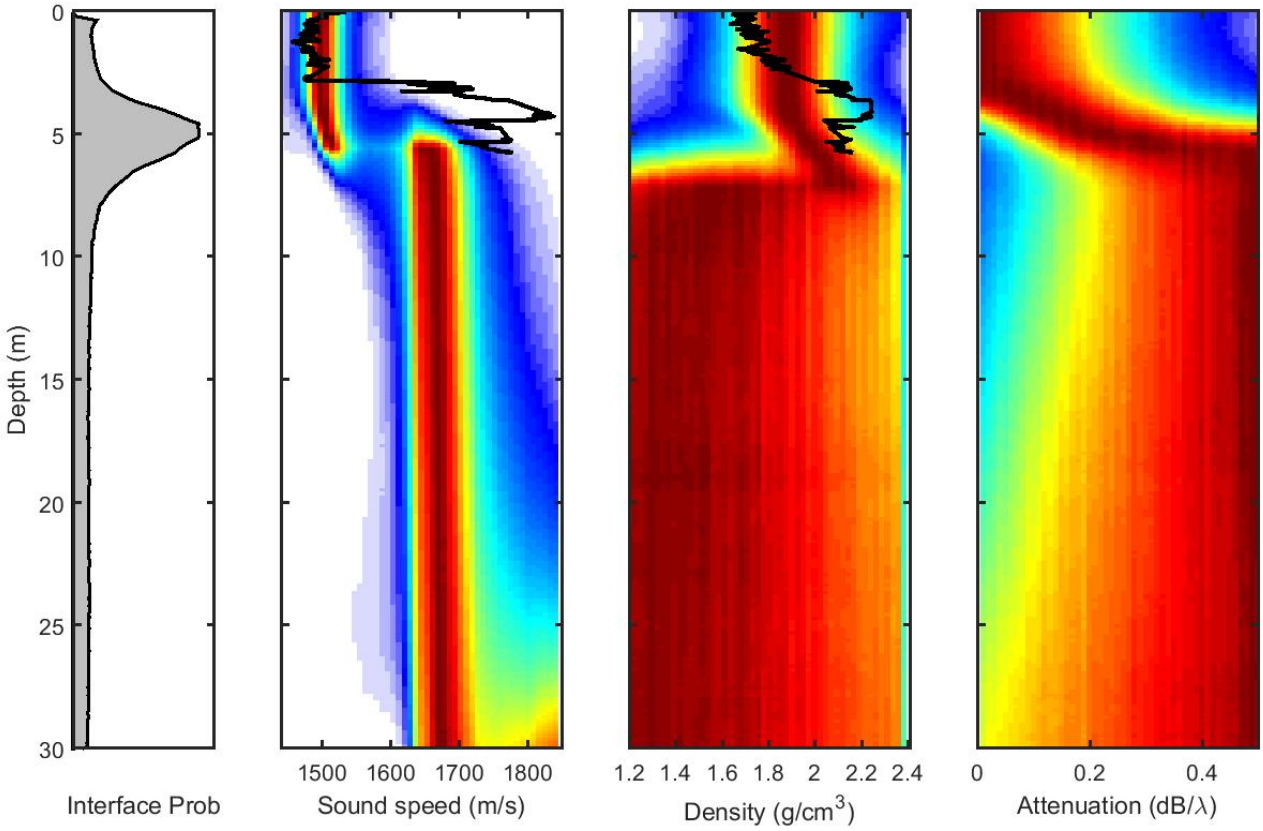

Fig. 11. Marginal posterior probability profiles for interface depth, sound speed, density, and attenuation. Four data segments, range 2.61–3.22 km, stern aspect. The black lines indicate the piston core 43PC analysis results.

D. Geometric parameters

Fig. 12 shows marginal probability densities for the geometric parameters, for the stern aspect (upper), bow aspect (middle), and first segment of the multiple segment inversion (lower distributions), respectively. For all parameters the plot bounds correspond to the prior bounds. Water depth (D) is distributed broadly within the prior bounds, with mean/mean-deviation estimates 66.8±0.8 m, 66.8±0.7 m, and 67.3±0.6 m, respectively, slightly less than the value of 68.6 m at the array location from the bathymetry model. Source depth (z) is distributed over 3–9 m, with mean/mean-deviation estimates 6.3±0.7 m, 5.9±1.0 m, and 6.2±0.5 m, respectively, consistent with the Gray-Greeley model value of 5.8 m for the noise-generating upper tip of the propeller for this ship. Source range (dr) is broadly distributed within the prior bounds. (The broad distributions can be due to a range/water depth ambiguity inherent in matched-field inversions, and due to ship movement over the time extent of a data

Dette er en postprint-versjon/This is a postprint version.
DOI til publisert versjon/DOI to published version: 10.1109/JOE.2019.2908026

segment.) Source bearing ($d\theta$) is sharply peaked with mean values (–47.3°, 44.0°, and –42.5°, respectively) in agreement with the nominal bearings.

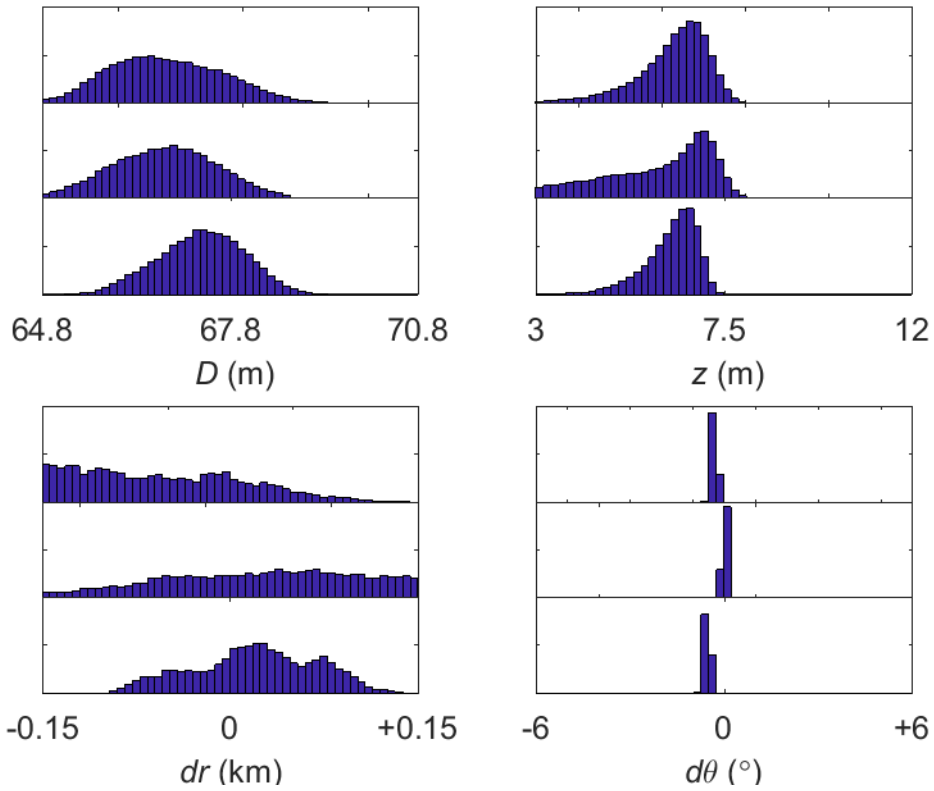

Fig. 12. Marginal probability distributions for geometric parameters for stern aspect (upper distributions), bow aspect (middle distributions), and first segment of multiple-segment (lower distributions) data.

E. Comparison with geophysical data

The ship noise inversion results in all cases clearly indicate an upper layer of low sound speed with small uncertainties that agrees reasonably well in thickness with the mud unit between the seafloor and mud base of the Goff *et al.* [14] sediment model for the New England Mud Patch. The thickness of this unit is not clearly resolved, but a transition to a higher speed layer is indicated between 3–7 m. The depth estimate (3–7 m) is in reasonable agreement with the surficial (fine-grained) sediment layer thickness at the array site of 4.5–6 m inferred from subbottom profiling data (Sec. II).

The sound speed value in the upper part of the seabed is in good agreement with core geophysical data collected in the area: the median sound speed of 1486 m/s in the upper 2 m of sediment from piston

Dette er en postprint-versjon/This is a postprint version.
DOI til publisert versjon/DOI to published version: 10.1109/JOE.2019.2908026

cores 43PC and 41PC agrees with the inversion result within its uncertainties (1508±22 m/s, at 0 m depth). The higher sound speed value at a greater depth (1678 m/s, but with considerable uncertainties to higher values) is in approximate agreement with core 43PC measurements (1745 m/s in the higher-speed layer). These higher sound speeds are consistent with deeper coarse-grained sediments (e.g., sand) in the Goff *et al.* [14] model.

The sound speed ratio between surficial sediments and the bottom of the water column is 1.026±0.015. In terms of the 95% highest probability density credibility interval, the inversion yields a sound speed ratio of 0.997–1.064. This does not exclude a sound speed ratio below 1.0; however, most of the probability is concentrated at sound speed ratios slightly above unity.

Internal layering of the mud unit is not resolved over the upper few meters in the ship-noise inversions, nor do the inversion results suggest a gradient in sound speed over these depths. However, the transition between the upper and lower sediment types is not clearly resolved: one inversion result (single data-segment stern aspect data) suggests a possible positive gradient near the bottom of the mud, while in the other two results the transition appears more abrupt. This uncertainty of the transition may be due to the limited information content of ship noise data. It may also due to possibly complicated depth-dependent structure of this transition in the sediments, and to variability in the transition depth with range along the tracks.

It is interesting to note the correspondence of high probabilities of sound-speed transition in the inversion results from about 3–7 m with the increase in sound speed measured for the piston core 43PC (Fig. 11). In particular, the core indicates a fairly abrupt increase in sound speed from approximately 1480 m/s to 1680 m/s at about 3 m depth, followed by a more gradual increase then variability over the next 2.5 m to the bottom of the core. The transition depth indicated from the core measurements is, however, less than the upper layer thickness of 5–7 m inferred from Fig. 1 for the core site; this may in part be due to unknown disturbances in the coring process.

The relatively high density values in the upper part of the seabed (1.89±0.16 g/cm^3, at 0 m depth) are also in agreement with core geophysical data (the median density from 43PC is 1.74 g/cm^3 in the upper

DOI til publisert versjon/DOI to published version: 10.1109/JOE.2019.2908026

2 m). Densities below the transition region are undetermined. Attenuation values are poorly constrained in the upper region, although one inversion suggests a relatively low attenuation (with large uncertainties); below the transition attenuations are undetermined. These results are likely due to limited information content for density and attenuation in low-frequency, long-range ship noise data.

V. SUMMARY

This paper applied trans-D matched-field geoacoustic inversion to noise from a commercial ship-of-opportunity received on a horizontal array on the seabed. Data were collected during the SBCEX17 experiment in the New England Mud Patch, a shallow water area with predominantly fine-grained (i.e., mud) upper sediment. Inversion results were obtained here using noise due to a container ship (frequencies 180–290 Hz) in passage near a HLA (480-m length, 20-element) on the seabed.

Results were generally consistent between inversions of three data sets: pre-CPA/bow aspect (range 4.07 km) and post-CPA/stern aspect (range 2.80 km) single segment data, and multiple-segment stern aspect data (range 2.61–3.22 km). In general, the inversions indicated seabed structure consisting of a homogeneous low sound speed upper sediment layer extending to 3–7 m depth over a higher-speed layer, with indication of a transition layer above the interface. Density and attenuation were largely unconstrained by the data, although relatively high density (and low attenuation) was indicated in upper sediment. Relatively wide prior bounds were applied to model geometric parameters (water depth and the position of a point source). These parameters were, except for source range, reasonably well constrained by the data. The peak of the posterior source depth distribution was in good agreement with the Gray-Greeley ship source depth model.

The parameter estimates for sediment sound speed and density in upper sediment were in good agreement with measurements of sound speed and density in the upper 2 m of two piston cores. The estimated sound speed ratio slightly above 1.0 at the water-sediment interface is indicative of fine-

DOI til publisert versjon/DOI to published version: 10.1109/JOE.2019.2908026

grained sediment (i.e., mud) in the upper seabed. Sound speed estimates indicated coarse-grained sediment (i.e., sand) in the lower seabed. This is in good overall agreement with the Goff *et al.* [14] sediment model based on subbottom profiling and coring data from the New England Mud Patch.

ACKNOWLEDGMENT

Support for this work was provided by the Office of Naval Research Code 32, Ocean Acoustics Program, and by the Office of Naval Research Global. The authors wish to thank the crew of the R/V *Neil Armstrong*, and the FFI engineering team.

REFERENCES

[1] D. J. Battle, P. Gerstoft, W. S. Hodgkiss, W. A. Kuperman, and M. Sideruis, "Geoacoustic inversion of tow-ship noise via near-field─matched-field processing," IEEE J. Ocean Eng. **28**, 454–467 (2003).

[2] M. Nicholas, J. S. Perkins, G. J. Orris, L. T. Fialkowski, and G. J. Heard, "Environmental inversion and matched-field tracking with a surface ship and L-shaped receiver array," J. Acoust. Soc. Amer. **116**, 2891–2901 (2004).

[3] R. A. Koch and D. P. Knobles, "Geoacoustic inversion with ships as sources," J. Acoust. Soc. Amer. **117**, 626–637 (2005).

[4] D. Tollefsen and S. E. Dosso, "Bayesian geoacoustic inversion of ship noise on a horizontal array," J. Acoust. Soc. Amer. **124**, 788–795 (2008).

[5] R. Koch, "Proof of principle for inversion of vector sensor array data," J. Acoust. Soc. Amer. **128**, 590–599 (2010).

[6] C. Gervaise, B. G. Kinda, J. Bonnel, Y. Stéphan, S. Vallez, "Passive geoacoustic inversion with a single hydrophone using broadband ship noise," J. Acoust. Soc. Amer. **131**, 1999–2010 (2012).

[7] D. P. Knobles, "Maximum entropy inference on seabed attenuation parameters using ship radiated broadband noise," J. Acoust. Soc. Amer. **138**, 3563–3575 (2015).

[8] J. E. Quijano, S. E. Dosso, J. Dettmer, L. M. Zurk, M. Siderius, and C. H. Harrison, "Bayesian geoacoustic inversion using wind-driven ambient noise," J. Acoust. Soc. Amer. **131**, 2658–2667 (2012).

[9] L. Muzi, M. Siderius, and C. M. Verlinden, "Passive bottom reflection-loss estimation using ship noise and a vertical line array," J. Acoust. Soc. Amer. **141**, 4372–4379 (2017).

[10] P. S. Wilson and D. P. Knobles, "Overview of the seabed characterization experiment 2017," in Proc. UACE2017 – 4th Underwater Acoustics Conference and Exhibition, 743-748, ISSN 2408-0195 (2017).

[11] J. Dettmer, S. E. Dosso, and C. W. Holland, "Trans-dimensional geoacoustic inversion," J. Acoust. Soc. Amer. **128**, 3393–3405 (2010).

[12] J. Dettmer and S. E. Dosso, "Trans-dimensional matched-field geoacoustic inversion with hierarchical error models and interacting Markov chains," J. Acoust. Soc. Amer. **132**, 2239–2250 (2012).

[13] S. E. Dosso, J. Dettmer, G. Steininger and C. W. Holland, "Efficient trans-dimensional Bayesian inversion for geoacoustic profile estimation," Inverse Problems **30**, 114018, 29 pp. (2014).

[14] J. A. Goff, J. D. Chaytor, A. H. Reed, S. Liu, P. S. Wilson, and D. P. Knobles, "The coarse-to fine-grained boundary beneath the New England Mud Patch: evidence from seismic and core data for an abrupt post-transgressive change in hydrologic regime on the continental shelf," American Geophysical Union, Fall General Assembly 2016, abstract id. EP24B-01 (2016).

[15] J.D. Chaytor, M. S. Ballard, B. Buczkowski, J. A. Goff, K. Lee, A. Reed, "Measurements of Geologic Characteristics, Geophysical Properties, and Geoacoustic Response of Sediments from the New England Mud Patch," in preparation for IEEE J. Ocean Eng. (2018).

[16] A. Reed and E. Braithwaite, "P-wave velocity and Density Core Logging – Leg I and II of the ONR NEMP Characterization: 2016," presented at the pre-experiment Workshop IV on the Seabed Characterization Experiment 2017, Arlington, VA, 6-8 June 2016, unpublished.

[17] P. T. Arveson and D. J. Vendittis, "Radiated noise characteristics of a modern cargo ship," J. Acoust. Soc. Amer. **107**, 118–129 (2000).

[18] D. K. Wittekind, "A simple model for the underwater noise source level of ships," J. Ship Prod. Des., **30**, 1–8 (2014).

[19] P. Zakarauskas, S. E. Dosso, and J. A. Fawcett, "Matched-field inversion for source location and optimal equivalent bathymetry," J. Acoust. Soc. Amer. **100**, 1493–1500 (1996).

[20] L. M. Gray and D. S. Greeley, "Source level model for propeller blade radiation for the world's merchant fleet," J. Acoust. Soc. Amer. **67**, 516–522 (1980).

[21] S. C. Wales and R. M. Heitmeyer, "An ensemble source spectra model for merchant-ship generated noise," J. Acoust. Soc. Amer. **111**, 1211–1231 (2002).

[22] E. K. Westwood, C. T. Tindle, and N. R. Chapman, "A normal mode model for acousto-elastic ocean environments," J. Acoust. Soc. Amer. **100**, 3631–3645 (1996).

[23] C. A. Zala and J. M. Ozard, "Matched-field processing for a moving source," J. Acoust. Soc. Amer. **92**, 403–417 (1992).

[24] P. J. Green, "Reversible jump Markov chain Monte Carlo computation and Bayesian model determination," Biometrika **82**, 711–732 (1995).

[25] W. R. Gilks, S. Richardson S, and G. J. Spiegelhalter, *Markov Chain Monte Carlo in Practice* (London: Chapman and Hall) (1996).

[26] M. Sambridge and K. Mosegard, "Monte Carlo methods in geophysical inverse problems," Reviews of Geophysics **40**, 3-1 3-29 (2002).

[27] A. Malinverno, "Parsimonious Bayesian Markov chain Monte Carlo inversion in nonlinear geophysical problems," Geophys. J. Int., **151**, 675–688 (2002).

[28] M. Sambridge, K. Gallagher, A. Jackson, and P. Rickwood, "Trans-dimensional inverse problems, model comparison and the evidence," Geophys. J. Int., **167**, 528–542 (2006).

[29] G. Steininger, J. Dettmer, S. E. Dosso, and C. W. Holland, "Trans-dimensional joint inversion of seabed scattering and reflection data," J. Acoust. Soc. Amer. **133**, 1347–1357 (2013).

[30] C. J. Geyer, "Markov chain Monte Carlo maximum likelihood" in Computing Science and Statistics: Proceedings of the 23rd Symposium on the Interface, p. 156–164 (1991).

[31] D. J. Earl and M. W. Deem, "Parallel tempering: Theory, applications, and new perspectives," Phys. Chem. Chem. Phys. **7**, 3910–3916 (2005).

[32] S. E. Dosso, C. W. Holland, and M. Sambridge, "Parallel tempering in strongly nonlinear geoacoustic Inversion," J. Acoust. Soc. Amer. **132**, 3030–3040 (2012).

[33] M. Sambridge, "A parallel tempering algorithm for probabilistic sampling and multimodal Optimization," Geophys. J. Int. **196**, 357–374 (2014).

[34] S. E. Dosso, P. L. Nielsen, and M. J. Wilmut, “Data error covariance in matched-field geoacoustic inversion,” J. Acoust. Soc. Amer. **119**, 208–219 (2006).

TABLES

TABLE I
CONTAINER SHIP TECHNICAL INFORMATION
FROM: www.marinetraffic.com, [a]AIS MESSAGE, [b]www.evergreen-line.com

Description and units	
IMO number	9629031
Gross tonnage (T)	99,946
Draft (m)[a]	11.8
Maximum draft (m)	14.2
Length overall (m)	335
Breadth extreme (m)	45.8
Maximum capacity (TEU)[b]	8508
Year built	2013

TABLE II
DATA SEGMENTS, TIME, NOMINAL RANGE, BEARING, AND SHIP ASPECT ANGLE.

Data Segment	Time (UTC)	Range (km)	Bearing (° *re* broadside)	Aspect angle (° *re* bow)
B1	065600	4.07	44.2	319
S1	070430	2.61	−43.0	228
S2	070500	2.80	−47.2	224
S3	070530	3.01	−50.8	220
S4	070600	3.22	−54.0	218

Dette er en postprint-versjon/This is a postprint version.
DOI til publisert versjon/DOI to published version: 10.1109/JOE.2019.2908026

TABLE III
SEABED PARAMETERS AND UNITS, PRIOR INFORMATION (SEARCH BOUNDS), AND INVERSION PARAMETER MEAN AND MEAN-DEVIATION UNCERTAINTY ESTIMATES AT DEPTHS 0 m, 5 m, AND 10 m, FOR STERN AND BOW ASPECT (SINGLE-SEGMENT) AND MULTIPLE-SEGMENT STERN ASPECT SHIP-NOISE DATA INVERSIONS. THE UNITS FOR ATTENUATION ARE DECIBELS PER ACOUSTIC WAVELENGTH λ.

Parameters and units	Prior Bounds	Depth (m)	STERN 2.80 km	BOW 4.09 km	MULTIPLE STERN 2.61–3.22 km
Sound speed (m/s)	1440–1850	0 5.0 10.0	1526±33 1581±53 1678±53	1511±34 1631±85 1705±58	1508±22 1584±67 1678±37
Density (g/cm^3)	1.2–2.4	0 5.0 10.0	1.98±0.20 1.97±0.23 1.83±0.30	1.80±0.21 1.77±0.27 1.66±0.29	1.89±0.16 1.89±0.21 1.74±0.29
Attenuation (dB/λ)	0–0.5	0 5.0 10.0	0.25±0.11 0.27±0.11 0.27±0.12	0.27±0.11 0.29±0.11 0.28±0.12	0.16±0.09 0.27±0.11 0.30±0.11

DOI til publisert versjon/DOI to published version: 10.1109/JOE.2019.2908026